This article has been accepted for publication in IEEE/OSA Journal of Lightwave Technology. This is the author's version which has not been fully edited and content may change prior to final publication. Citation information: DOI 10.1109/JLT.2021.3095522

60 GHz Resonant Photoreceiver with an Integrated SiGe HBT Amplifier for Low Cost Analog Radio-Over-Fiber Links

Nishant Singh, Guy Torfs, Joris Van Kerrebrouck, Christophe Caillaud, Piet Demeester, and Xin Yin.

***Abstract*—An analog radio-over-fiber photoreceiver based on a resonant narrowband transimpedance low noise amplifier (TILNA) is proposed and demonstrated for use in low-cost and low-power remote radio heads for distributed antenna systems in the unlicensed 60 GHz band. The amplifier is designed to present a conjugate matched impedance to a wirebonded photodiode where the input impedance has a real part of 10Ω while the output impedance is matched towards 50Ω. Fabricated in a 55nm SiGe BiCMOS technology, the TILNA features a three stage common emitter low noise amplifier with 17 dB of gain, a 3.4 dB noise figure, an output 1-dB compression point of 8 dBm and low power consumption of 33.6 mW while occupying only 0.25 mm^2 of chip space including pads. The photoreceiver, formed by the TILNA and a wirebonded InP UTC photodiode, offers 29 dB higher gain than a 50Ω terminated reference photodiode where 11 dB improvement is provided by resonant matching. Experimental results show that the proposed photoreceiver has achieved up to 20 Gbps C-band transmission of complex modulated waveforms over 5 km of standard single-mode fiber using 4 Gbaud QAM32 with an RMS EVM of 11.5%.**

***Index Terms*—BiCMOS integrated circuits, Microwave photonics, Microwave amplifiers, Millimeter wave radar, Millimeter wave communication.**

I. Introduction

THE V-band around 60 GHz has been allocated for unlicensed use across most of the world and is considered a high priority millimeter wave band by a majority of the industry [1], [2]. Organizations such as the WiFi alliance and 3GPP have incorporated this band into their standards with the WiFi alliance including it in IEEE 802.11ad/ay and 3GPP recently deciding to extend 5G new radio (NR) frequency range 2 (FR2) to 71 GHz [3], [4]. 3GPP is in the process of finalizing waveforms and numerology and is expected to formally include it in release 17 in 2022 where it may be used to augment licensed access (NR-U-LAA) or as a standalone network (NR-U-SA). This is the first cellular standard ever to include unlicensed standalone operation, consequently, NR-U-SA is a competitor to WiFi and has the potential to provide a unified single wireless networking standard. Moreover, radar systems operating at 60 GHz have become mainstream with almost all major chipmakers offering solutions. Similar to the communications application domain, multiple antenna and distributed systems are being utilized in next generation demonstrators [5].

A big issue with moving to mmWave frequencies is the higher path loss therefore multiple distributed antenna units are needed to provide coverage to an area and it is preferable to consolidate baseband units (BBU) and share capacity across remote radio heads (RRH) [6], [7]. Typically, digital optical fiber links carrying common public radio interface (CPRI) data have been used to connect BBUs to RRHs as shown in Fig. 1 [7].

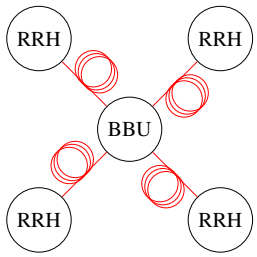

Fig. 1: Distributed antenna system with optical fiber transport.

A typical radio-over-fiber (RoF) downlink is shown in Fig. 2 where a signal is converted from the electrical to the optical domain (E/O) and back from optical to the electrical domain (O/E). The common RoF implementation utilizes digital radio-over-fiber (DRoF) to carry CPRI data but this requires complex RRHs. Intermediate frequency-over-fiber (IFoF) has been promoted as a lower cost solution compared to DRoF but it requires upconversion at the RRH [8]. Sigma-delta radio-over-fiber (SDMRoF) proposes a simple RRH architecture but has only been demonstrated up to 28 GHz [6]. Analog radio-over-fiber (ARoF) using optical single sideband (OSSB) modulation has been demonstrated as a preferred solution for large scale mmWave deployments due to elimination of dispersion induced power fading while offering a simple RRH architecture [9].

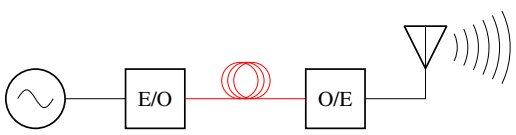

Fig. 2: A radio-over-fiber downlink.

This work was supported in part by the ERC Advanced Grant ATTO Project under Grant 695495 and in part by H2020 5G-PHOS Project under Grant 761989. (Corresponding author: Nishant Singh)

Nishant singh, Guy Torfs, Joris Van Kerrebrouk and Xin Yin are with the IDLab, Department of Information Technology, Ghent University - imec, B-9052 Ghent, Belgium, e-mail: (see https://www.ugent.be/ea/idlab/en/members).

Christophe Caillaud is with III-V Lab, F-91767 Palaiseau, France.

Manuscript received March 15, 2021; revised May 31, 2021; acepted June 21, 2021, date of curent version July 6, 2021.

This article has been accepted for publication in IEEE/OSA Journal of Lightwave Technology. This is the author's version which has not been fully edited and content may change prior to final publication. Citation information: DOI 10.1109/JLT.2021.3095522

Different ARoF photoreceivers exist for mmWave frequencies however they are made in costly III-V technologies which have low yield and scale poorly for mass production due to small wafer sizes [10], [11], [12]. A low cost solution has to be realized in high performance technologies that are cheap to mass produce and should be assembled in cost effective ways. SiGe BiCMOS is a good candidate for RFICs as it offers heterojunction bipolar transistors (HBTs) with f_T/f_{max} above 300 GHz and a favorable copper back-end-of-line (BEOL) metal stack with metal-insulator-metal (MIM) capacitors [13].

This paper is an extension of our ECOC2020 paper and demonstrates a narrowband photoreceiver consisting of a SiGe BiCMOS amplifier and an InP UTC photodiode connected using wirebonds [14]. The photoreceiver exhibits 29 dB higher gain than a reference photodiode over a 3 dB bandwidth of 5.7 GHz while consuming 33.6 mW, 17 dB of the gain improvement is due to amplifier gain while 11 dB due to resonant matching. There is 2 dB of combined loss in the input wirebonds the output probe while the reference photodiode has 3 dB loss at 60 GHz. In section II, the gain increase owing to resonant matching is discussed. Section III further extends on the design of the amplifier and its standalone measurements. Section IV discusses the measurements of the assembled photoreceiver. Section V concludes this paper.

II. Concept and Motivation

In order to efficiently extract mmWave power from a photodiode (PD) and amplify it with minimal added noise, a transimpedance low noise amplifier (TILNA) is proposed for use in a narrowband photoreceiver (NBPhoRx) operating at 60 GHz as shown in Fig. 3. The TILNA is designed to present a conjugate matched load to the photodiode which is a low impedance source while the output impedance is 50 Ω towards further components in the RF chain such as an antenna or a power amplifier.

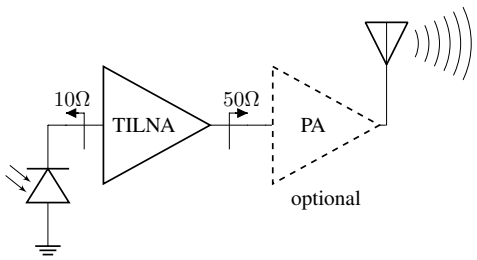

Fig. 3: A narrowband photoreceiver (NBPhoRx) using a transimpedance low noise amplifier (TILNA).

To allow high bandwidth, a InP uni-traveling-carrier (UTC) PD was used and its impedance in reverse bias was characterized using on-wafer 1-port vector network analyzer (VNA) measurements. A smith chart representation of the S_{11} is shown in Fig. 4. A narrowband lumped model can be extracted from the S_{11} measurements for 60 GHz and is shown in Fig. 5 (a). A current source represents the current generated when optical power is incident on the junction, this can be transformed to a Thevenin equivalent circuit as show in Fig. 5 (b). The power extracted if the load impedance is conjugate of the source impedance can be seen in (1). An analytical expression for matched gain when compared to a lossless 50Ω terminated PD is shown in (2). This is 11 dB for our PD which is a significant improvement and justifies the design of a dedicated amplifier.

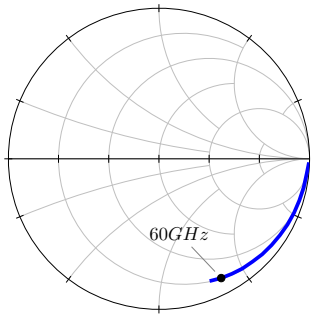

Fig. 4: S_{11} of photodiode measured using a standard 50Ω VNA from 1 GHz to 67 GHz.

$$P_L = \frac{I_{rms}^2}{4\omega^2 C_S^2 R_S} \tag{1}$$

$$Gain = \frac{1}{50\omega^2 C_S^2 R_S} \tag{2}$$

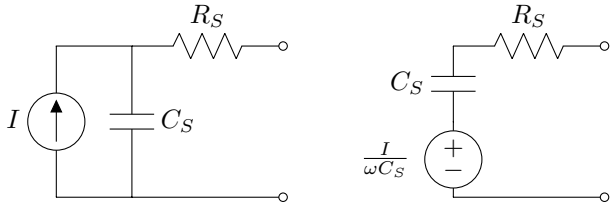

Fig. 5: Narrowband equivalent circuit at 60 GHz of (a) a photodiode (b) its Thevenin equivalent.

III. TILNA

The TILNA consists of three low noise gain stages as shown in Fig. 6. This shows only real parts of the impedances as the reactive parts of the impedances are canceled in interstage matching networks. The input impedance of the first stage is 10Ω and its output impedance is 30Ω. This stage is optimized for low noise with sufficient gain. The second stage has an input and output impedance of 30Ω, this stage is optimized for medium noise and high gain. The third stage has an input impedance of 30Ω while the output impedance is 50Ω, this stage is optimized for high gain and linearity. A simplified schematic of the TILNA is shown in Fig. 7.

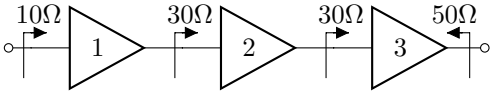

Fig. 6: Overview of TILNA stages

This article has been accepted for publication in IEEE/OSA Journal of Lightwave Technology. This is the author's version which has not been fully edited and content may change prior to final publication. Citation information: DOI 10.1109/JLT.2021.3095522

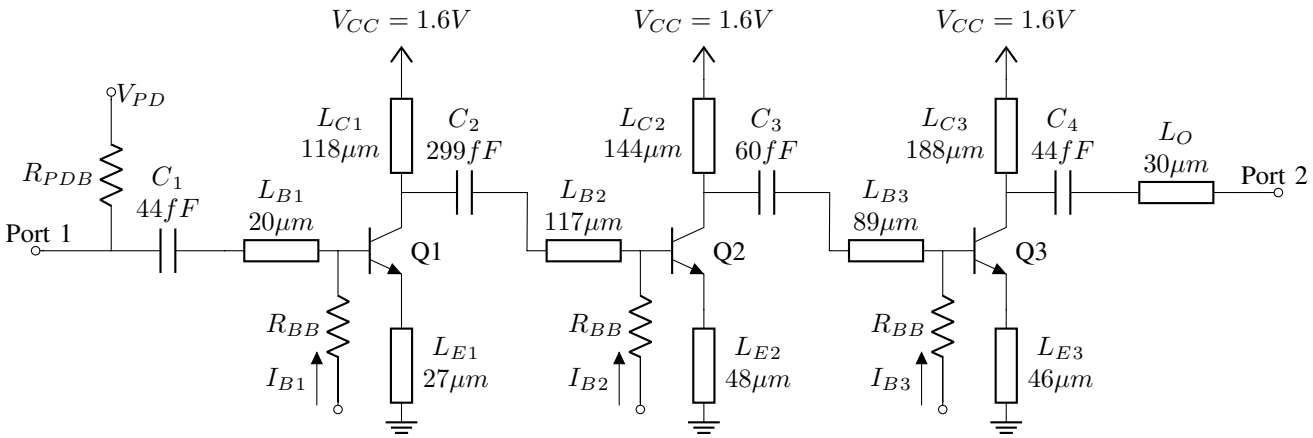

Fig. 7: Simplified schematic of TILNA.

There will be some integration parasitics originating from bondwires or an interposer. These must be taken into account as part of the input network as shown in Fig. 8. The first stage shall accommodate all interconnect and minimize extra matching networks that will increase loss. Any mismatch or loss before the first stage will have a dominant contribution to the overall noise figure (NF) of the amplifier.

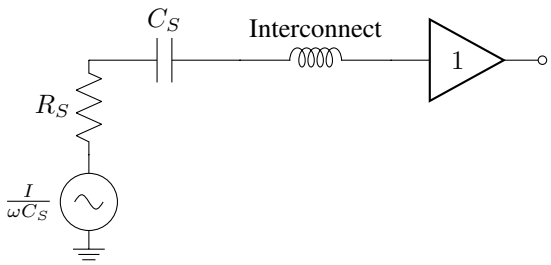

Fig. 8: Simplified schematic of input network.

The low noise gain stages are realized using HBTs in a common emitter (CE) configuration with emitter degeneration. Inductive elements are realized in thick top metal using $0.6\mu m$ width lines with exceptions L_{B1} $2\mu m$ and L_O $14.4\mu m$. Capacitive elements are realized using MIMs while high ohmic polysilicon resistors are used for biasing networks.

The input stage transistor $Q1$ is sized for optimum source noise impedance (Z_{sopt}) equal to the real part of the PD impedance and biased through a base resistor R_{BB} for a collector current I_{C1} close to minimum noise figure (NF_{min}) while providing sufficient gain. The real part of the input impedance (Z_{in}) of this stage is also designed to be equal to the real part of the PD impedance using an emitter inductor L_{E1}. The base inductor L_{B1} is sized to remove imaginary components of Z_{in} and Z_{sopt}. The collector inductor L_{C1} is sized for output impedance of 30 Ω. The capacitor C_2 provides output matching and DC decoupling. It is sized to tune out the imaginary component of the output impedance (Z_{out}) of this stage. The second and third stages are designed in a similar manner. The HBT $Q1$ is larger than $Q2$ and $Q3$ as it has a very low Z_{sopt} and therefore requires a higher current for a similar current density. $Q1$ is biased at an I_{C1} of 9 mA while $Q2$ and $Q3$ are biased with I_{C2} of 5 mA and I_{C3} of 7 mA. This totals to a current consumption of 21 mA from a 1.6 V source for a power consumption of 33.6 mW.

The photodiode is biased through an on-chip bias tee comprising of a capacitor C_1 and a resistor R_{PDB}. The capacitor in this bias tee is sized to resonate out a portion of the bondwire inductance. The resistor should be sized to handle the expected DC photocurrent while providing sufficient AC decoupling. An on-chip power supply decoupling was implemented using a large array of MIM capacitors (omitted from schematic). A total of 29 MIM capacitors with values of 1.6 pF were used for a total decoupling capacitance of 46.4 pF. Collector inductors were retuned to compensate for the effect of the decoupling network. Ground-signal-ground (GSG) pads with a size of 40 x 60 and a pitch of 150 μm were used for RF interfaces and their models included in respective networks.

The TILNA was manufactured on a commercial 55nm SiGe BiCMOS process and characterized with a VNA using wafer probes calibrated to probe tips. DC bias was provided using wirebonds. A micrograph of the TILNA under test is shown in Fig 9.

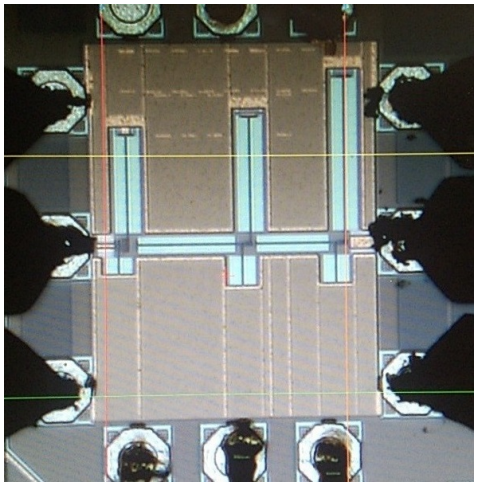

Fig. 9: Micrograph of TILNA under test.

While the VNA measures the two-port using 50 Ω ports, the measured S-parameters can be translated to the port

This article has been accepted for publication in IEEE/OSA Journal of Lightwave Technology. This is the author's version which has not been fully edited and content may change prior to final publication. Citation information: DOI 10.1109/JLT.2021.3095522

impedances expected in the design. As such, the system performance with integration parasitics can be simulated using a testbench as shown in Fig. 10. The output was designed to accommodate flip-chip assembly which is represented by the 90 pH inductance at output. This is missing in the wirebond assembly and will cause about 1 dB of output probing losses. The S_{21} is shown in Fig. 11 indicating 17 dB of gain while S_{11} and S_{22} are shown in Fig. 12 confirming matching. A power sweep was also conducted with the VNA and is shown in Fig. 13 with an OP1dB of 8 dBm.

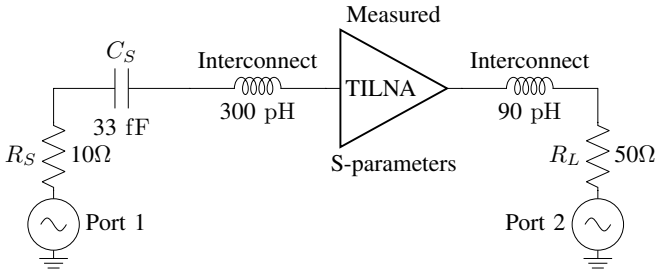

Fig. 10: Simulation testbench for extracting matched gain of TILNA from VNA measurements.

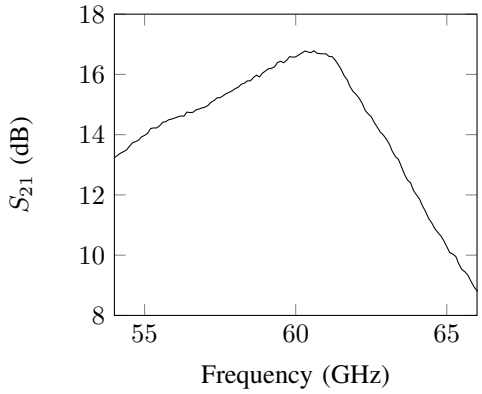

Fig. 11: Matched gain of TILNA.

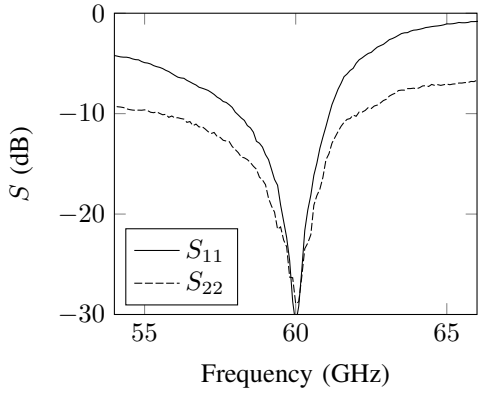

Fig. 12: Input and output reflection response of TILNA.

IV. NBPhoRx Assembly and Experimental Results

The PD and TILNA were assembled together on a PCB and connected using wirebonds as shown in Fig. 14. The critical

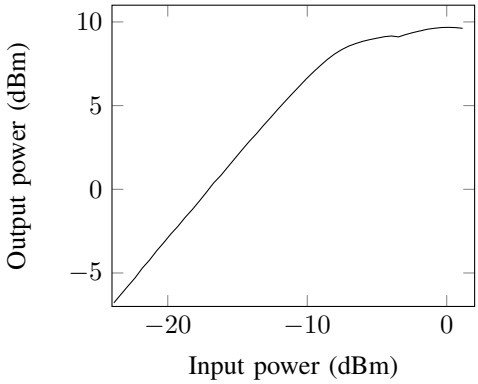

Fig. 13: Gain compression of TILNA

wirebonds between the PD and TILNA were formed using ball-stitch-on-ball (BSOB) shapes while DC was provided using ball-stitch shapes. The input was interfaced with a lateral fiber probe while output was accessed through GSG probes. The performance of the NBPhoRx in an optical link was characterized using a measurement setup as shown in Fig. 15 which was later extended for link experiments as shown in Fig. 16.

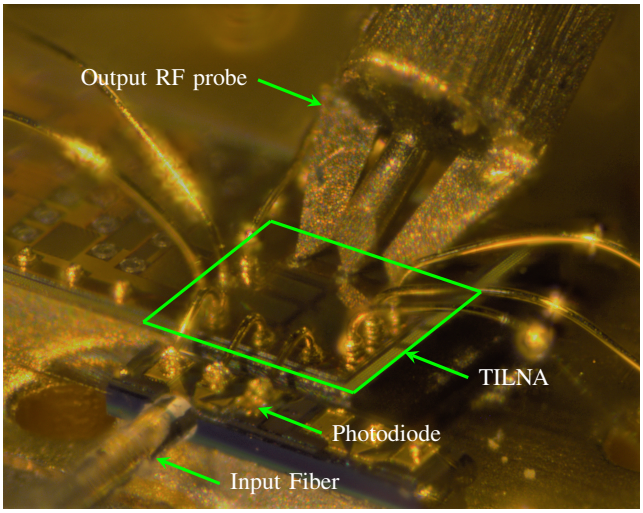

Fig. 14: Macrograph of NBPhoRx under test showing optical input fiber edge coupling and RF output probing.

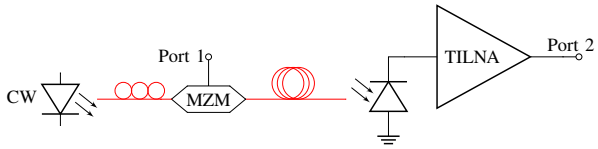

Fig. 15: Two port VNA measurement setup for NBPhoRx.

The link was set up using a commercial laser (Tunics T100S-HP) and a Mach-Zehnder modulator (MZM, Fujitsu FTM7937EZ) biased at quadrature at an optical wavelength of 1550 nm. The VNA was connected at ports 1 and 2 as indicated in the diagram and calibrated to the end of its cables. As such, the output probe was included in the

This article has been accepted for publication in IEEE/OSA Journal of Lightwave Technology. This is the author's version which has not been fully edited and content may change prior to final publication. Citation information: DOI 10.1109/JLT.2021.3095522

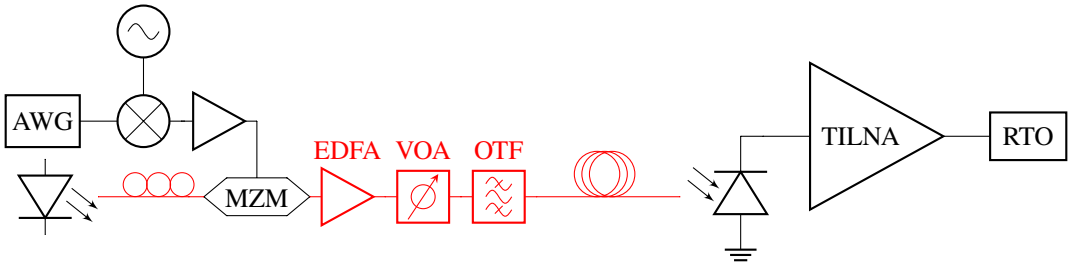

Fig. 16: Experimental setup for RoF downlink using NBPhoRx.

measurements. A reference PD (Finisar XPDV2120-RA) was used to characterize the frequency response of the transmitter and to de-embed the characteristic of the NBPhoRx. The de-embedded frequency response of the NBPhoRx in an optical back-to-back (B2B) scenario can be seen in Fig. 17. The NBPhoRx is characterized to have a 29 dB gain at the center frequency with a 3 dB bandwidth of 5.7 GHz. Of the 29 dB gain, 17 dB is from active TILNA gain while 11 dB is from resonant matching. There is 2 dB of loss combined in the RF probe and input wirebonds while there is 3 dB of loss in the reference PD.

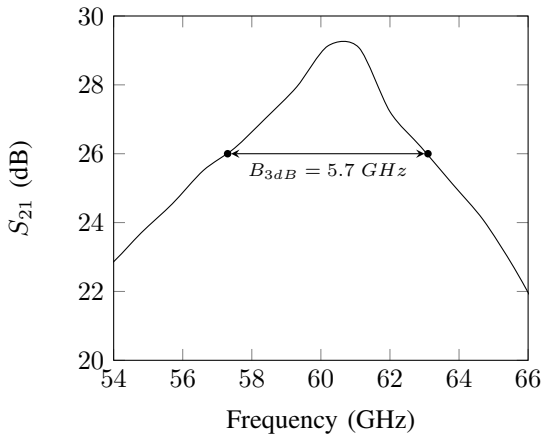

Fig. 17: Transmission response of NBPhoRx.

As shown in Fig. 16, a RoF downlink setup was built to demonstrate transmission of complex modulated waveforms using the NBPhoRx. The VNA measurement setup from Fig. 15 was extended by placing a transmitter at port 1 and a receiver at port 2. The output probe and cable to the receiver were not calibrated out and form part of the link. The transmitter comprises an arbitrary waveform generator (AWG, Keysight M8195A), an oscillator (Anritsu MG3696B), a mixer (VDI WR12eCCU) and three cascaded amplifiers (SHF M827B). The received signal from the NBPhoRx was demodulated with a real time oscilloscope (RTO, Keysight DSAZ634A).

The single carrier waveforms were generated with the AWG at an IF frequency of 11 GHz and upmixed to 60 GHz using a passive mixer and a LO of 35.5 GHz as the mixer module includes an LO frequency doubler. To overcome the insertion loss of the mixer, three amplifiers were used to amplify the low power (-30 dBm) signal to drive the MZI modulator with a signal power of 0 dBm which corresponds to 0.6 V V_{pp}. This limited the measurement as the V_{pi} of the modulator in single drive is 3.6 V. Furthermore, the optical 3 dB bandwidth of the MZM is 25 GHz and it exhibits 9 dB of loss at 60 GHz. Due to the high loss and low diving voltage, the modulation depth of the test transmitter was very poor at 14% and the optical power contained in a sideband of the modulated signal at the output of the MZM was -40 dBm. This caused a very high DC current through the on-chip PD bias-tee in the NBPhoRx while signal power was very low.

In order to improve the modulation depth and the side band power, an Erbium-doped fiber amplifier (EDFA, Keopsys CEFA-C-HG) with an optical tunable filter (OTF, Santec OTF-350) was used with a variable optical attenuator (VOA, Keysight N7762A) in the middle to control the power coming from the EDFA. The OTF was used to filter out some of the carrier power and one of the sidebands. This increased the power contained in the sideband at the output of the OTF to -20 dBm. The filtering of a sideband also had the added benefit of converting the optically modulated signal to OSSB which eliminated dispersion induced power fading. This signal was transmitted over 5 km of standard single mode fiber (SSMF) to the NBPhoRx.

The output of the NBPhoRx was connected to a RTO using a 0.5 m RF cable which has 7 dB loss. The signals were demodulated in realtime on the RTO using vector signal analysis (VSA) digital demodulation software with built-in adaptive 21-tap finite impulse response (FIR) equalizer to compensate for the gain roll off. The equalizer was run initially to adapt filter shape to minimize reference EVM after which the shape was held at those values. The obtained constellations are shown in Fig. 18. It can be seen the data rates of up to 20 Gbps are demonstrated at a symbol rate of 4 Gbaud using QAM32 at an EVM of 11.5%. For reference, the EVM was measured at the transmitter after the RF amplifier and was found to be 4%. The link experiment was limited by the availability of transmit side components and has room for improvement. A comparison of the TILNA with the state-of-the-art can be seen in Table I. It can be seen that this implementation is very compact and has low power consumption while offering good performance.

V. Conclusion

This work proposes and demonstrates an ARoF NBPhoRx for the unlicensed 60 GHz V-band based on a TILNA. The TILNA is designed to have a low input impedance to conjugate match the PD while the output impedance is 50Ω. The TILNA

TABLE I: Comparison with the state-of-the-art

	Process Technology	Frequency	Amplifier Gain	NF	OP1dB	Size	Power Consumption
This Work	55nm SiGe BiCMOS	60 GHz	17 dB	3.4 dB*	8 dBm	0.25 mm^2	33 mW
[10]	0.1μm GaAs pHEMT	28 GHz	24 dB	2 dB	9.7 dBm	4.76 mm^2	160 mW
[11]	GaAs HEMT	60 GHz	24 dB	4 dB	17.5 dBm	-	965 mW
[12]	0.1μm AlGaAs pHEMT	93 GHz	22 dB	-	7.8 dBm	11.2 mm^2	219 mW

*Simulated

(a) (b)

Fig. 18: Obtained constellations for QAM32 over 5 km SSMF (a) 1 Gbaud with EVM of 9% and (b) 4 Gbaud with EVM of 11.5%.

was manufactured in a commercial 55nm SiGe BiCMOS process and characterized to have 17 dB gain with 33.6 mW power consumption. The TILNA and PD were assembled on a PCB and electrically connected using wirebonds to form the NBPhoRX. The NBPhoRx has 29 dB higher gain than a reference photodiode of which 11 dB can be attributed to resonant matching. The NBPhoRx is demonstrated with complex modulated waveforms at data rates up to 20 Gbps over 5 km SSMF with a QAM32 modulated signal at 4 Gbaud with an EVM of 11.5%.

ACKNOWLEDGMENT

The authors would like to thank Michal Szaj at Argotech for the wirebonding service, Laurens Breyne for the PCB, Luc Pauwels and Nele Van Hoovels for help during probing and Xavier Allart from Keysight Technologies for assistance during measurements.

REFERENCES

[1] R. C. Daniels and R. W. Heath, "60 GHz wireless communications: Emerging requirements and design recommendations," *IEEE Vehicular Technology Magazine*, vol. 2, no. 3, pp. 41–50, Sep. 2007.

[2] Intel Corporation, "Summary of Rel-17 email discussion on NR above 52.6GHz," 3GPP, Document RP-191914, Sept. 2019.

[3] N. Patriciello, S. Lagen, B. Bojovic, and L. Giupponi, "NR-U and IEEE 802.11 Technologies Coexistence in Unlicensed mmWave Spectrum: Models and Evaluation," *IEEE Access*, pp. 1–1, 2020.

[4] Qualcomm, "New WID on Extending current NR operation to 71 GHz," 3GPP, Document RP-193229, Dec. 2019.

[5] A. Kanno, T. Umezawa, T. Kuri, N. Yamamoto, T. Kawanishi, and Y. N. Wijayanto, "Key technologies for millimeter-wave distributed RADAR system over a radio over fiber network," in *2016 International Conference on Radar, Antenna, Microwave, Electronics, and Telecommunications (ICRAMET)*, 2016, pp. 1–6.

[6] C. Wu, H. Li, J. Van Kerrebrouck, A. Vandierendonck, I. L. de Paula, L. Breyne, O. Caytan, S. Lemey, H. Rogier, J. Bauwelinck, P. Demeester, and G. Torfs, "Distributed Antenna System Using Sigma-Delta Intermediate-Frequency-Over-Fiber for Frequency Bands Above 24 GHz," *Journal of Lightwave Technology*, vol. 38, no. 10, pp. 2765–2773, 2020.

[7] G. Giannoulis, N. Argyris, N. Iliadis, G. Poulopoulos, K. Kanta, D. Apostolopoulos, and H. Avramopoulos, "Analog Radio-over-Fiber Solutions for 5G Communications in the Beyond-CPRI Era," in *2018 20th International Conference on Transparent Optical Networks (ICTON)*, 2018, pp. 1–5.

[8] A. Matera, R. Kassab, O. Simeone, and U. Spagnolini, "Non-Orthogonal eMBB-URLLC Radio Access for Cloud Radio Access Networks with Analog Fronthauling," *Entropy*, vol. 20, no. 9, 2018.

[9] Y. Tian, K. Lee, C. Lim, and A. Nirmalathas, "60 GHz Analog Radio-Over-Fiber Fronthaul Investigations," *Journal of Lightwave Technology*, vol. 35, no. 19, pp. 4304–4310, 2017.

[10] L. Bogaert, H. Li, K. Van Gasse, J. Van Kerrebrouck, J. Bauwelinck, G. Roelkens, and G. Torfs, "36 Gb/s Narrowband Photoreceiver for mmWave Analog Radio-over-Fiber," *Journal of Lightwave Technology*, pp. 1–1, 2020.

[11] S. Fedderwitz, C. C. Leonhardt, J. Honecker, P. Muller, and A. G. Steffan, "A high linear and high power photoreceiver suitable for analog applications," in *IEEE Photonics Conference 2012*, 2012, pp. 308–309.

[12] T. Umezawa, K. Kashima, A. Kanno, A. Matsumoto, K. Akahane, N. Yamamoto, and T. Kawanishi, "100-GHz Fiber-Fed Optical-to-Radio Converter for Radio- and Power-Over-Fiber Transmission," *IEEE Journal of Selected Topics in Quantum Electronics*, vol. 23, no. 3, pp. 23–30, 2017.

[13] P. Chevalier, W. Liebl, H. Rucker, A. Gauthier, D. Manger, B. Heinemann, G. Avenier, and J. Bock, "SiGe BiCMOS Current Status and Future Trends in Europe," in *2018 IEEE BiCMOS and Compound Semiconductor Integrated Circuits and Technology Symposium (BCICTS)*, 2018, pp. 64–71.

[14] N. Singh, J. van Kerrebrouck, C. Caillaud, P. Demeester, X. Yin, and G. Torfs, "60 GHz Resonant Photoreceiver with an Integrated SiGe HBT Amplifier for Analog Radio-over-Fiber Links," in *2020 European Conference on Optical Communications (ECOC)*, 2020, pp. 1–4.